Numerical study of the wall shear stress produced by the impingement of a plane turbulent jet on a plate

Received June 1995
Revised October 1996

M. Bouainouche, N. Bourabaa and B. Desmet
LAMIH-Conception des Systèmes Mécaniques et Energétiques, Valenciennes, France

Nomenclature

A	=	coefficients of discretized equations
$C\mu$	=	turbulence-model constant
e	=	jet gap
E	=	roughness parameter
H	=	nozzle-to-plate distance
$k = u_i^2/2$	=	turbulent kinetic energy
l	=	turbulence length scale
L_m	=	mixing length
p	=	pressure
P_k	=	rate of production of turbulent kinetic energy
Pe	=	Peclet number
$Re_0 = U_0 e/\nu$	=	Reynolds number
$Re_t = \rho k^{1/2} l/\mu = \nu t/\nu$	=	turbulent Reynolds number
S_ϕ	=	source term of ϕ equation
T	=	temperature
u	=	fluctuating velocity
U	=	mean velocity in x-direction
$U^+ = U_p/U_\tau$	=	non-dimensional value of U_P
$U_\tau \sqrt{\tau_w/\rho}$	=	friction velocity
V	=	mean velocity in y-direction
$\vartheta = \Delta x.\Delta y.1$	=	control volume
x, y	=	co-ordinates
$y^+ = U_\tau y_P/\nu$	=	non-dimensional value of y_P

Greek symbols

χ	=	von Karman constant
$\Delta x, \Delta y$	=	mesh lengths
$\varepsilon = \nu(\partial\overline{U_i}/\partial x_j)^2$	=	turbulent kinetic energy rate of dissipation
ϕ	=	dependent variable
Γ_ϕ	=	diffusion coefficient of variable ϕ
ν	=	kinematic viscosity
$\nu_t = C_\mu k^2/\varepsilon$	=	turbulent kinematic viscosity
ρ	=	density
τ	=	shear stress
$\Psi = k^{1/2}/U_\tau$	=	non-dimensional value of $k^{1/2}$

Subscripts

0	=	values at nozzle exit
i, j	=	tensor notation
n	=	values at node points: N, S, W and E.
P	=	values at node point P
w	=	wall values

Note: The symbols defined above are subject to alteration on occasion

Introduction

The topic of this paper is the wall function influence on the results of computation of the wall shear stress produced by a normal impinging thin plane turbulent jet on a flat plate. This study is justified by the necessity to possess data that will be used for the analysis of jets and liquid deposits interaction problems. Some engineering problems can be noted e.g. jet-blast drying and coating thickness control.

International Journal of Numerical Methods for Heat & Fluid Flow
Vol. 7 No. 6, 1997, pp. 548-564.

Some researchers[1-3] have experimentally studied the impingement of turbulent jets on a solid surface and have established some empirical laws giving velocity, pressure and shear stress distributions along the flat wall.

The authors generally divide the jet flow field into three fundamental regions (Figure 1): I is referred to as the free jet region, II is the impingement region and III is the wall jet region. The experimental study[2] is used as a specific reference to validate calculations. Other authors have studied this problem using numerical methods[4-8]. In all these studies, the classical wall logarithmic law is used. In discretization schemes, the first grid point must be located at the beginning of the logarithmic region, just outside the viscous sub-layer. Looney and Walsh[7] have used the generalized form of the logarithmic law to predict the shear stress in the impingement region.

As a closure model, most studies use the standard k-ε turbulence model. Recently, Leschziner[6] has found that the Reynolds stress model is superior to the k-ε model only in the case of a swirling jet and in a large recirculation flow region. In the case of a plane jet impinging normally on a plate, the calculation results using either one of the two models are almost identical. By imposing a small mesh in the boundary layer, the RSTM model generates a slow calculation. For this reason, the high Reynolds number k-ε turbulence model was chosen with the wall functions in this work. The influence of these wall laws over the shear stress calculation is studied in detail here. To minimize the influence of the near wall grid on the prediction of the shear stress, a hybrid wall law is proposed. A "choice criterion" for the near wall grid is defined. Calculations are validated through experimental data.

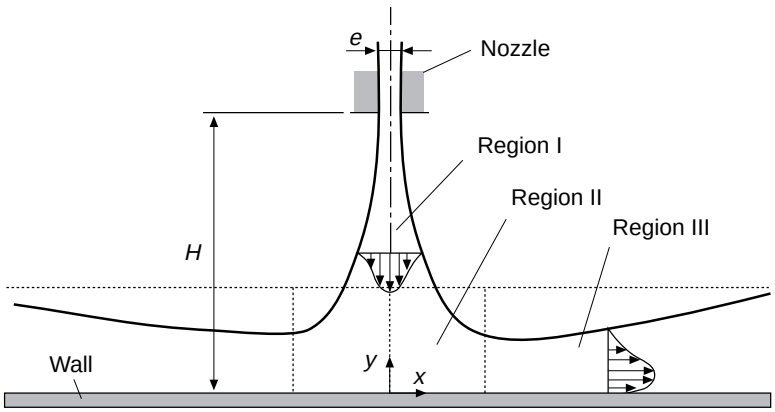

Figure 1.
Impinging jet system

Mathematical model

Conservation equations

The flow of a turbulent jet impinging on a plate is governed by continuity, momentum and energy equations. The equations of turbulent kinetic energy k and the rate of dissipation ε, which represent the standard k-ε turbulence model[9], are added to the previous equations. For a steady two-dimensional flow, these equations can be written with the following general conservation form:

$$\underbrace{\frac{\partial}{\partial x}(\rho U \phi) + \frac{\partial}{\partial y}(\rho V \phi)}_{\text{Convective term}} = \underbrace{\frac{\partial}{\partial x}\left(\Gamma_\phi \frac{\partial \phi}{\partial x}\right) + \frac{\partial}{\partial y}\left(\Gamma_\phi \frac{\partial \phi}{\partial y}\right)}_{\text{Diffusive term}} + \underbrace{S_\phi}_{\text{Source term}} \quad (1)$$

Resolution procedure

By using the finite volume scheme[10], the calculation domain is discretized into a computational mesh. Equation (1) is integrated over the finite control volume (Figure 2) ensuring the preservation of the conservation properties. The result is a set of equations having the following form:

$$A_P \phi_P = \sum_n A_n \phi_n + b$$

where A are coefficients representing convection and diffusion contributions, b the integrated source term, and $\sum_n$ the summation over node P's four neighbouring nodes.

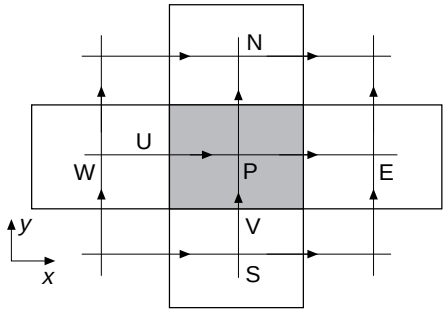

Figure 2.
Volume control of calculation

The SIMPLEST algorithm, the modified version of SIMPLE proposed by Patankar[11], is used to solve the coupling between continuity and momentum equations through pressure. A hybrid differencing scheme combining the advantages of both upwind and central differencing is used to ensure stability at all values of Peclet number and to limit the effects of numerical diffusion. Since the iterative method is used, the initial conditions corresponding to the variables must therefore be specified. For a steady flow, these conditions do not affect the final result but only the convergence velocity.

In order to take into account the external shape of the nozzle, a quasi-orthogonal mesh is used in the whole flow domain, except near the flat plate. The influence of the nozzle external shape on the flow will be presented later. On the other hand, the Cartesian mesh is adopted near the wall. Strong grid clustering is used at the impinging wall and at the jet axis. As the geometry to study is symmetrical in the case of a normal impinging jet, only half of the physical domain is solved. Different grids were tested to ensure independence from the numerical results on the grid density. A typical grid size of 60×27 ($\Delta x.\Delta y$) has been used in most of the solved cases. A typical grid is shown in Figure 3. All variables were converged after 2,000 iterations. In the first 500 iterations, the energy equation is not coupled with the other equations.

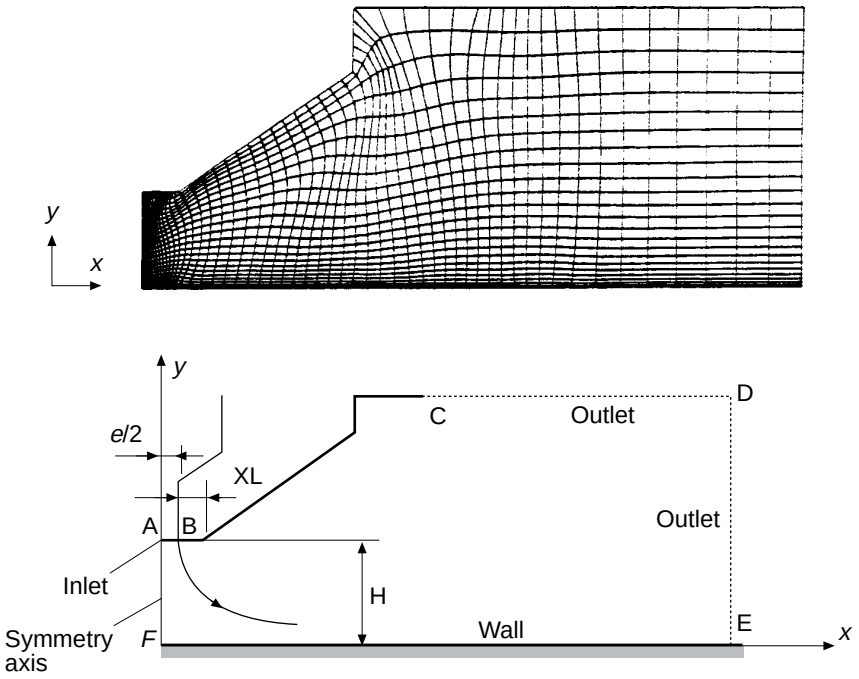

Figure 3.
Typical numerical grids and boundary conditions for calculation

Boundary conditions

The flow field ABCDEF in Figure 3 is selected as the domain of interest over which the governing differential equations are integrated. Four boundary condition types are used:

- Symmetry axis FA. The velocity component U and the gradients of the other dependent variables in the x direction are chosen equal to zero.
- "Outlet" conditions CD and DE at ambient pressure. The dependent variables gradients in the normal direction to the outlet boundary are set equal to zero.
- Wall conditions BC and EF representing the nozzle blowing external shape and the flat plate.
- Inlet conditions AB corresponding to the blowing section at the outlet of the nozzle.

The last two boundary condition types will be described in greater detail in the following sections.

Inlet conditions

The jet velocity V_0 and temperature T_0 are regarded as uniform at the nozzle exit i.e. the limit AB of the calculation domain. The turbulence properties k_0 and ε_0, are determined from the jet velocity[12] as follows:

$$k_0 = 0.04 V_0^2 \quad \text{and} \quad \varepsilon_0 = \frac{C_\mu^{3/4} k_0^{1.5}}{\ell}$$

The length scale of turbulence *l* at the inlet is set to 0.1 e.

Wall conditions

The standard k-ε model used in the present work is applicable only to flow regions with high turbulence Reynolds number Re_t. In the region near the wall, i.e. viscous sub-layer, the effect of molecular viscosity and turbulence Reynolds number is small. When the flow Reynolds number is high, the thickness of this region is very small and difficult to model. A precise calculation of the flow requires several discretization points in the viscous sub-layer and the intermediate zone where the velocity gradients are high. A practical method to solve this problem is to link up the model to a relation called the wall function or the wall law. The latter is established from empirical hypothesis and enables us to connect wall conditions to another calculation domain. In the field of the first grid point near the wall, where the convection is neglected as compared to the diffusion, the turbulence kinetic equation for a shear flow can be written in the form:

$$\mathrm{div}\left(\Gamma_k \overrightarrow{\mathrm{grad}}\, k\right) + S_k = 0 \tag{2}$$

The velocity component parallel to the wall at the first grid point U_p (Figure 4) and the turbulence kinetic energy k_p are assessed through numerical integration of the corresponding equations. The wall shear stress τ_w is deduced from the wall function. The equation of the kinetic energy rate of dissipation ε at the first grid point is not solved, but this rate is calculated from the relation[12]:

$$\varepsilon_P = \frac{C_\mu^{3/4} k^{3/2}}{\chi y} = \frac{U_\tau^3}{\chi y} \tag{3}$$

The classical logarithmic law and the generalized one are used subsequently to predict the friction along a smooth flat plate with the impinging jet on it. These laws are based on incompressible boundary layer approximations. However, an experiment of Chieng and Ng[13] in the case of a strongly heated boundary layer demonstrates that the logarithmic wall law is also convenient in the case of an expansive fluid.

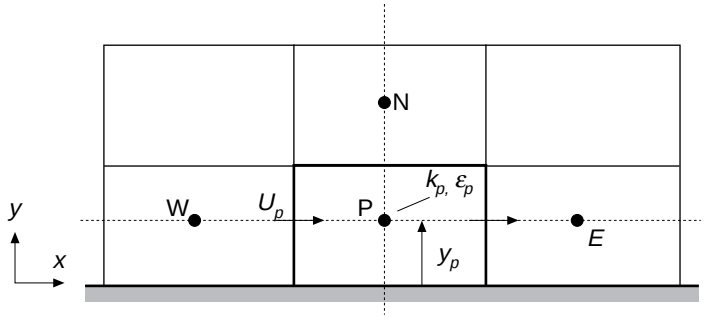

Figure 4.
First grid point near the wall

Logarithmic wall law

This law is associated with the mixing length hypothesis for a shear flow, where the turbulent viscosity is:

$$\nu_t = L_m^2 \left(\frac{\partial U}{\partial y} \right) \qquad \text{With } L_m = \chi\, y$$

Velocity at the first grid point near the wall (located outside the viscous sub-layer) is related to the wall shear stress by the logarithmic law:

$$-\overline{u_i u_j} = \frac{\tau}{\rho} \approx \frac{\tau_w}{\rho} = \chi^2 y^2 \left(\frac{\partial U}{\partial y} \right)^2$$

where $-\rho\overline{u_i u_j}$ denotes the Reynolds stresses since:

$$\frac{\partial U}{\partial y} = \frac{\sqrt{\tau_w / \rho}}{\chi\, y}$$

After integration, at each grid point, the velocity U_p in the high Reynolds number region according to a friction velocity U_τ formulation is written as follows:

$$U^+ = \frac{1}{\chi} \ln \left(E y^+ \right) \qquad \text{for } y^+ > 12 \tag{4}$$

In the viscous sub-layer:

$$U^+ = y^+ \qquad \text{for } y^+ \leq 12$$

χ = 0,41 and E = 9 for a smooth wall[12].

Constants χ and E are compatible with the constants of the k-ε turbulence model. This compatibility ensures the results' continuity at the boundary between the wall law and the internal points where the turbulence model is applicable. Turbulence kinetic energy k on this boundary is determined from a local equilibrium hypothesis between production and dissipation (source term is equal to zero). This hypothesis allows a linear link between the turbulence kinetic energy and the shear stress: $k_p = U_\tau^2 / \sqrt{C_\mu}$. Dissipation is furthermore linked to the shear stress and to the first grid point distance to the wall by the relationship (3).

Generalized wall law

Here, the local equilibrium between the production of turbulence kinetic energy and its dissipation is not prescribed. A generalization of the logarithmic wall law is obtained by taking the square root of the turbulence kinetic energy as the velocity scale[14]. Thus the turbulent viscosity near the wall is expressed in the following form:

$$\nu_t = \chi\, C_\mu^{1/4} k^{1/2} y$$

By using a similar development as for the classical logarithmic law, one obtains:

$$\frac{\partial U}{\partial y} = \frac{\sqrt{\tau_w/\rho}}{\chi^* k^{1/2} y}$$

After integration, a similar expression to the relation (4) with different normalization scales is found:

$$U^+ \psi = \frac{1}{\chi^*} \ln\left(E^* y^+ \psi\right) \tag{5}$$

where

$$\chi^* = \chi C_\mu^{1/4} \quad \text{and} \quad E^* = E C_\mu^{1/4}$$

It is necessary in this case to solve the turbulence kinetic energy equation; equation (2) is integrated over the control volume of Figure 4:

$$\int_\vartheta \operatorname{div}\left(\Gamma_k \vec{\operatorname{grad}}\, k\right) d\vartheta + \int_\vartheta S_k \, d\vartheta = 0 \tag{6}$$

The first term of relation (6) is integrated by assuming that there is no diffusion at the wall: $(\partial k/\partial y)_w = 0$. The second term is composed of the difference between averaged production and dissipation rates:

$$\overline{S_k} = \left(\overline{P_k} - \bar{\varepsilon}\right) \vartheta$$

The averaged production rate in the grid cell is:

$$\overline{P_k} = \frac{1}{\vartheta} \int_\vartheta -\overline{u_i u_j} \frac{\partial U}{\partial y} d\vartheta = \frac{U_\tau^2 U_P}{2 y_P} \tag{7}$$

The averaged dissipation rate in the grid cell is:

$$\bar{\varepsilon} = \frac{1}{\vartheta} \int_\vartheta \varepsilon \, d\vartheta = \frac{C_\mu \psi^3 U_\tau^3}{2 \chi^* y_P} \ln\left(E^* y_P^+ \psi\right) \tag{8}$$

The main use of this form of wall function is in flows with conditions far from the local equilibrium. However, it is widely used in finite volume schemes applied to recirculating and separated flows[15].

Results and discussion

Influence of the external shape of the nozzle on jet actions

To demonstrate the influence of the external shape of the nozzle on the jet actions[16], the flow is modelled for two lengths (XL = 5mm and XL = 20mm) of the nozzle end shown in Figure 3. For the two cases, distance H is set to 7.5mm and jet gap e to 1.0mm. Inlet velocity V_0 is chosen equal to 197m/s.

The pressure distributions (Figure 5) show negative values for the relative pressure when XL = 20mm. When the nozzle length XL is large, a swirling flow occurs in the region between the nozzle and the flat plate. Owing to the blockage produced by the recirculating zone, the velocity increases in the non-disturbed flow region. This increase of velocity can explain the negative values of the relative

pressure[5] and the higher values of the wall shear stress (Figure 5). The streamline analysis[16] shows that for XL = 5mm, the surrounding air goes along the external wall of the nozzle and is then dragged down by the jet towards the flat plate.

These results show that the influence of the external shape of the nozzle may be significant on the pressure and the wall shear stress values for small nozzle-to-plate distances. Therefore, the use of empirical relationships available in the references is not easy because the external shape of the nozzle is generally not defined.

Wall shear stress distribution along a plate

Distributions of shear stress along a flat plate caused by the impingement of a normal plane jet are studied. To validate computation results, the experimental configuration of Mohamed Aly[2] is used. Calculations are carried out for a length of the nozzle end XL equal to 5mm, an exit nozzle velocity of 190m/s and relative nozzle-to-plate distances H/e equal to 10, 15 and 25 with a 1mm jet gap e. Results shown in Figures 6 to 12 correspond to case $H/e = 25$.

This study aims at determining the influence of the distance of the first grid point y_p from the wall over values of the shear stress. The classical logarithmic and the generalized wall laws previously presented are used and the errors

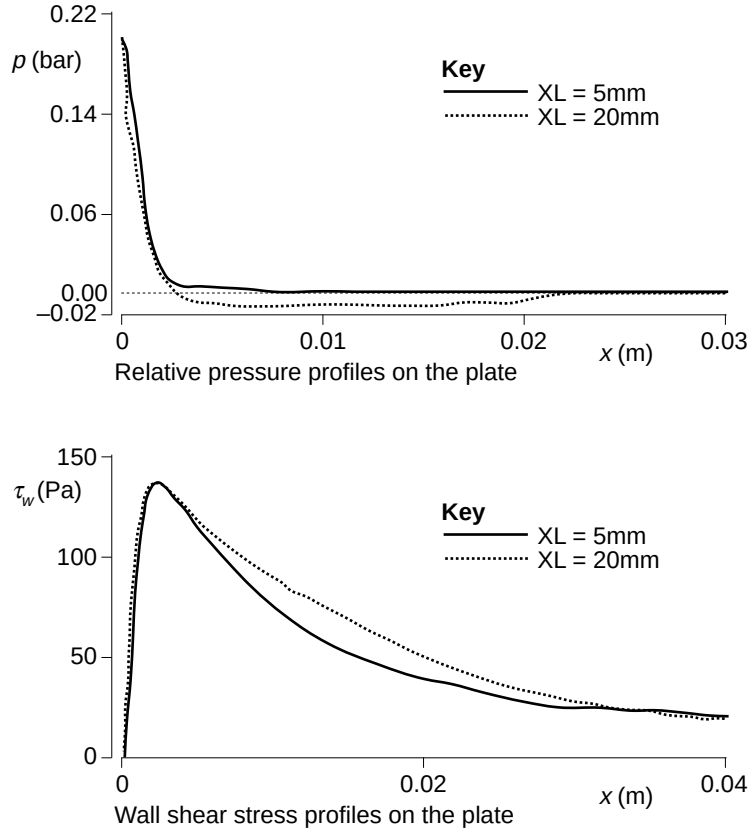

Figure 5.
Influence of the external shape nozzle (H = 7.5mm; e = 1mm; V_0 = 197m/s)

generated within the friction computations for each law are evaluated. Six calculations were carried out for each wall law with a relative distance of the first grid point from wall y_p/H varying from 0.0014 to 0.01.

Logarithmic law results. Figure 6 describes the wall shear stress distributions at different relative distances y_p/H, evaluated using the standard logarithmic law. The distribution shape is similar to the one measured[2]. After a zero value at the jet axis, the shear stress increases very quickly over a few millimetres until it reaches its peak in the impinging jet region, then it decreases slowly in the wall jet region. The shear stress is overestimated or underestimated depending on y_p/H value. It decreases when distance y_p/H increases.

Gaps between wall shear stress distributions in accordance with y_p/H values are of paramount importance in the vicinity of distribution law peak. These gaps decrease in the zone located in the vicinity of the jet axis and in the wall jet region. The best fit between the calculated value of the shear stress and the measured one is obtained with $y^+ = 30$ corresponding to $y_p/H = 0.002$. In this case, node P is located just outside the viscous sub-layer and at the beginning of the logarithmic region flow. But it is difficult to abide by this condition ($y^+ \approx 30$) before each calculation.

Generalized law results. Wall shear stress distributions on a flat plate are calculated from the generalized law and compared to experimental data. Figure 7 shows that in the impinging jet region, peak shear stress values are well predicted for different distances y_p/H except for the greatest value 0.01. On the other hand, just after the maximal point for $x > 5.5$mm corresponding to $x/H > 0.02$, the shear

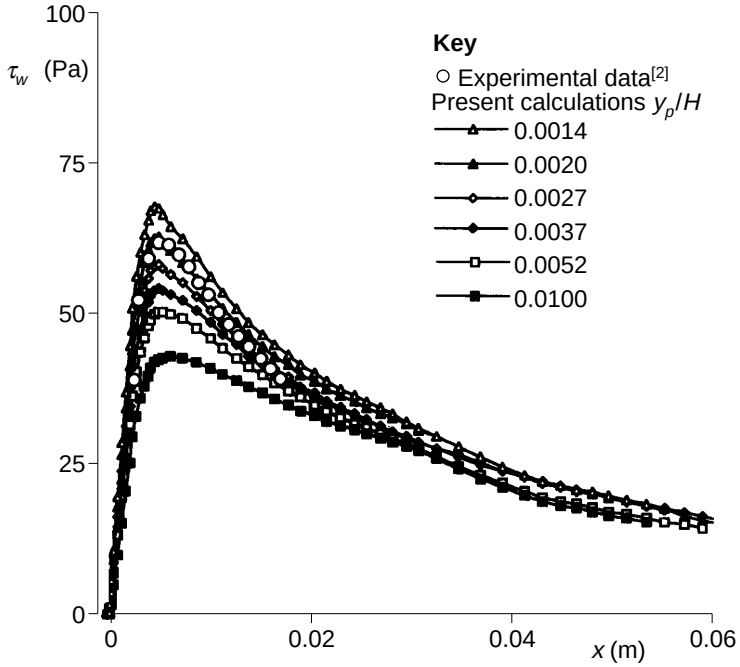

Figure 6.
Wall shear stress distribution for different y_p/H – logarithmic wall law is used

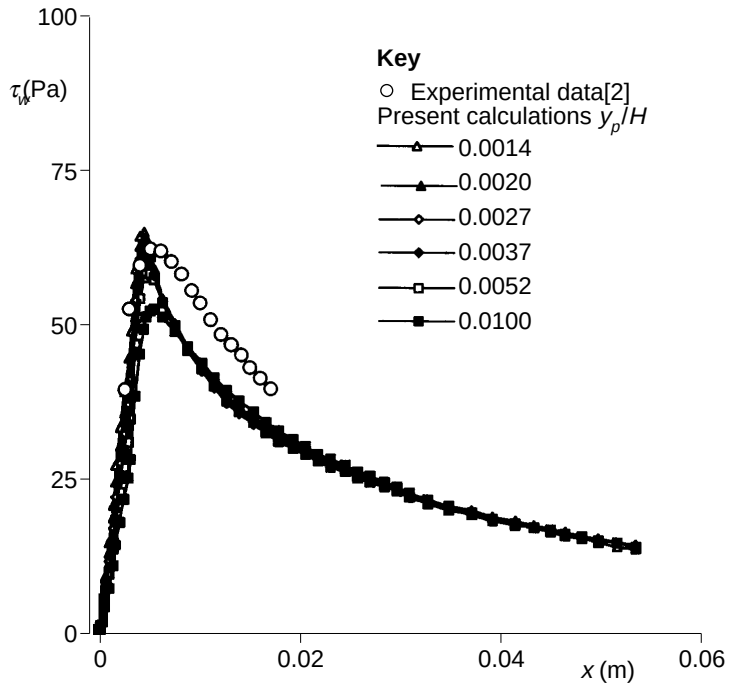

Figure 7.
Wall shear stress distribution for different y_p/H – generalized wall law is used

decreases very rapidly and values are identical in the wall jet region. These values are smaller than the experimental data in this region. The same verification is made by Looney and Walsh[7] using this type of wall law; their predictions are correct in the impingement region but they do not study the wall jet region.

To conclude, the generalized wall law gives a proper prediction of the wall shear stress up to the peak point in the impingement region but it has the disadvantage of underestimating the shear stress in the wall jet region.

Hybrid wall law. The main hypothesis of the generalized law is that of a lack of equilibrium between the production of turbulent kinetic energy and its dissipation, in contrast to the case of the standard logarithmic law. That encourages us to go further on to improve on that which was predicted. To collect information related to this last condition, profiles of the production rate of turbulent kinetic energy and its dissipation rate corresponding to relations (7) and (8), are shown in Figure 8. These profiles are like those of the wall shear stress and they are identical except for the following:

- in the vicinity of the peak, the values of the dissipation rate ε are higher than those of production rate P_k; and
- in the wall jet region the values of ε are lower than those of P_k.

Far from the jet axis, the two distributions vanish to zero. As shown subsequently, this configuration has some importance for the prediction of wall shear stress. These results prompt us to combine the two types of wall laws giving the so called “hybrid law”. The principles of the hybrid wall law are:

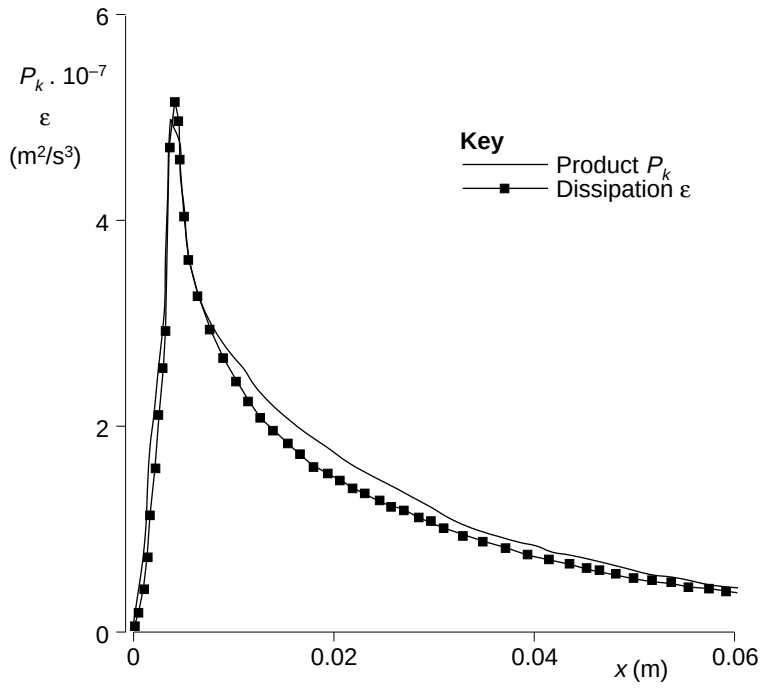

Figure 8.
Profiles of P_k and ε calculated by the generalized wall law

- In the impingement region, the generalized law suitably predicting the wall shear stress with less influence of the grid close to the wall on these calculations is used. The production rate of turbulent kinetic energy P_k is lower than the dissipation rate ε ($P_k/\varepsilon < 1$).
- In the wall jet region, the standard logarithmic law can be used to ensure the local equilibrium between production and dissipation rates of k ($P_k = \varepsilon$).

The transition between the two laws is defined at distance $x/H \approx 0.22$.

Figure 9 describes the production and dissipation rates distributions by using the hybrid law. The two profiles coincide everywhere except in the vicinity of the maximum values where the dissipation rate is higher than the production rate ($P_k/\varepsilon < 1$). In figures 10 and 11, where P_k and ε are plotted, both generalized and hybrid laws are compared. The difference between the two laws is visible in the region located just after the peak point and this difference is greater in the case of ε (Figure 11).

To assess performances of the hybrid law, the shear stress distributions are drawn by using the same values of y_p/H (ranging from 0.0014 to 0.01) for the logarithmic law (Figure 6) and the generalized law (Figure 7). Figure 12 shows an improvement of the calculation results: less difference between the different profiles on the peak values of shear stress as compared to Figure 6 (generalized law effect) and a progressive decrease after these values in the wall jet region (logarithmic law effect) are observed. For a good prediction of shear stress distribution along a plate a “choice criterion” is established and is defined by:

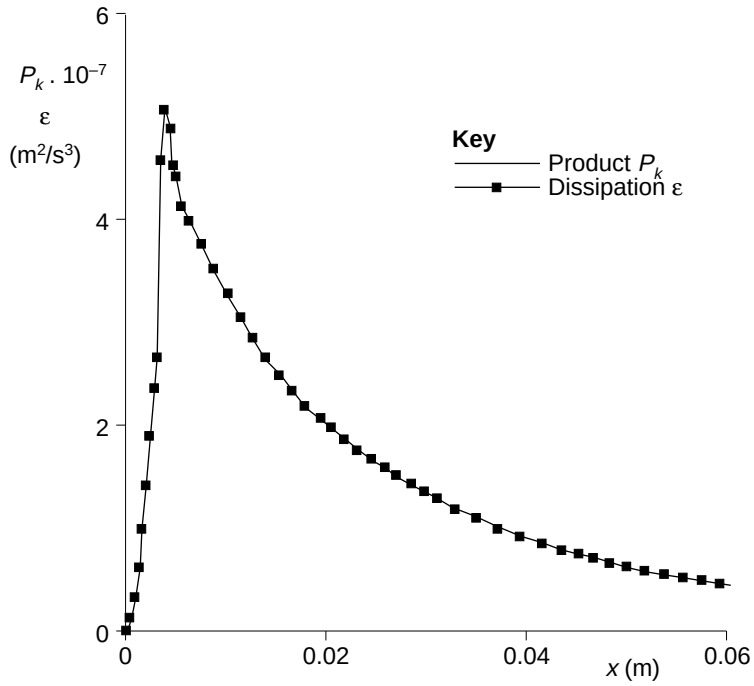

Figure 9.
Profiles of P_k and ε calculated by the hybrid wall law

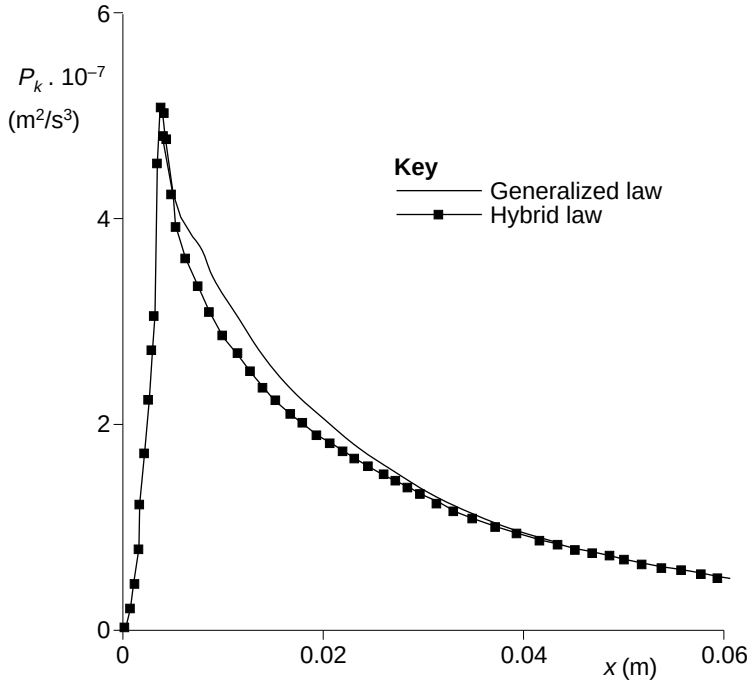

Figure 10.
Comparison of P_k between the generalized and the hybrid wall laws

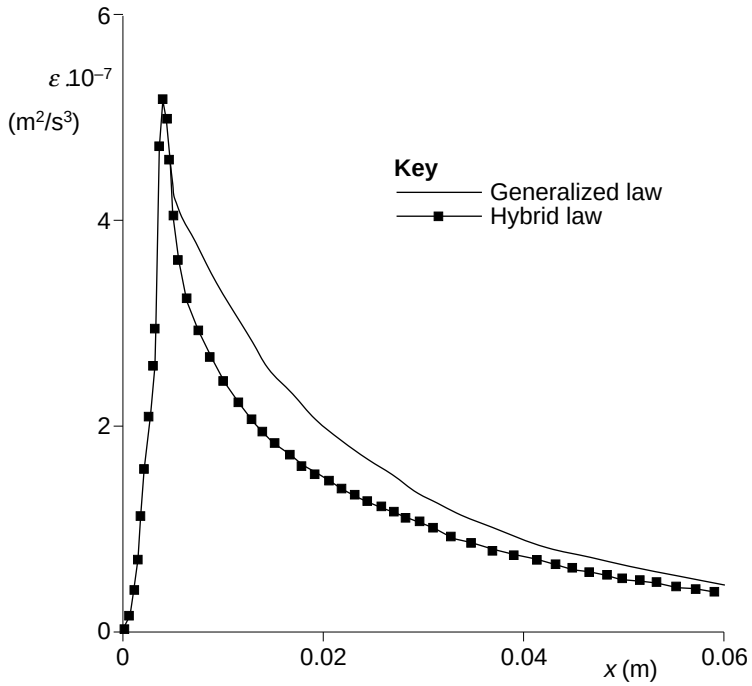

Figure 11.
Comparison of ε between the generalized and the hybrid wall laws

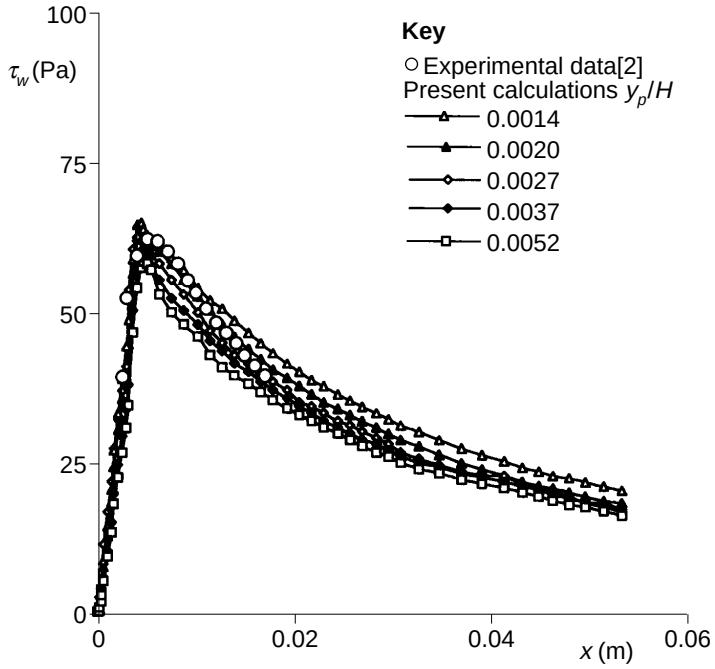

Figure 12.
Wall shear stress distributions – hybrid wall law is used

$$0.0014 \leq y_p/H \leq 0.0052 \quad (9)$$

A general comparison between profiles of wall shear stress calculated by hybrid, standard and generalized laws is presented in Figure 13. These results are given for a distance $y_p/H = 0.002$ for the three laws. Figure 14 compares the predictions of wall shear stress distributions corresponding to different values H/e (10, 15 and 25) with the experimental data available. The choice criterion (9) and the value $x/H \approx 0.22$, which is the transition between the two laws, are applied for these computations. For the peak values of wall shear stress, the non-dimensional variable y^+ must vary between 20 and 60. In the numerical study of wall jet, Ljuboja and Rodi[17] recommend the use of values between 30 and 60 for y^+.

Finally, in Figure 15, to ensure the validity of the present modelling, the friction velocity in the non-dimensional form $(U_\tau/V_0)(H/e)^{1/2}$ is plotted against x/H for calculation results using the hybrid law and experimental data of Beltaos and Rajaratnam[1] with $Re_0 = 7{,}100$ and $Re_0 = 5{,}680$ for $H/e = 66.15$, Mohamed Aly[2] with $Re_0 = 12{,}786$ for $H/e = 25$ and Shauer and Eustis[3] with $Re_0 = 43{,}000$ for $H/e = 40$. Comparisons show a good agreement between calculations and measurements even for high distance H/e and for high Reynolds number.

In these last experimental works, the Preston probe is used to measure the wall shear stress. It is important to specify that in the impingement region, large favourable pressure gradients are present and, based on the general recommendations of Patel[18], the possible error in the wall shear stress will be less than 6 per cent for $x/H > 0.225$ and could be larger in the immediate neighbourhood of the impingement point. Within the measurement errors, the agreement between calculation results and experimental data is suitable.

Pressure distribution along a plate

In addition to the wall shear stress, the impingement of a jet on a flat plate also causes a pressure distribution. Figure 16 compares the prediction of wall pressure distributions with experimental data[2] for relative distance H/e equal to 10, 15 and 25, and velocity at nozzle exit equal to 190m/s. A good agreement is found between prediction and measurement profiles. The value of pressure is maximal at the impingement point and very rapidly decreases to be subsequently cancelled in the wall jet region.

Conclusion

In this work, an optimization of the calculation of the jet flow impinging on a flat plate has been attempted. Special attention was focused on the wall shear stress evaluation. For a suitable calculation of this wall shear stress along a plate with less dependence on the grid close to the wall, a hybrid law is proposed. This law provides a more accurate prediction of the shear stress in the impingement region (generalized law effect) while keeping the advantage of the logarithmic law in the wall jet region.

For a good prediction of shear stress distributions on the plate, a “choice criterion” for the first grid point near the wall was established. This criterion

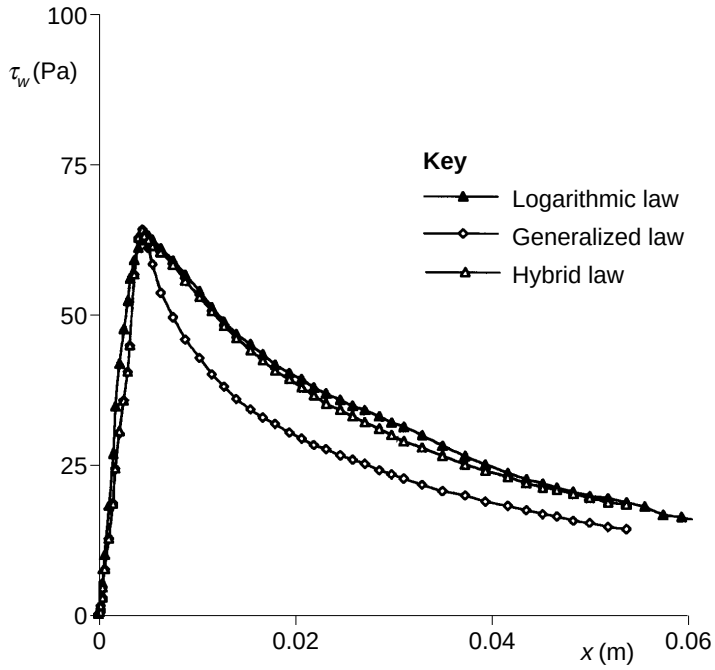

Figure 13.
Comparison between the wall laws – wall shear stress distributions

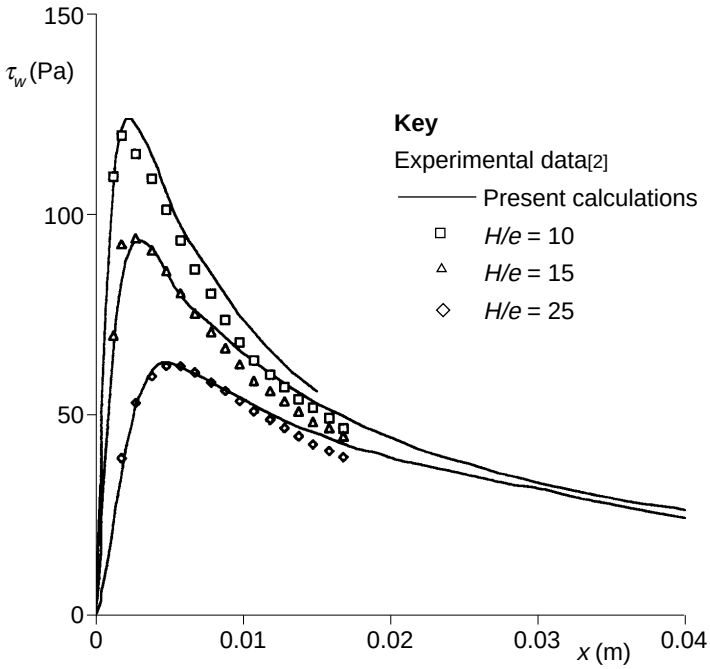

Figure 14.
Wall shear stress distribution calculated and measured

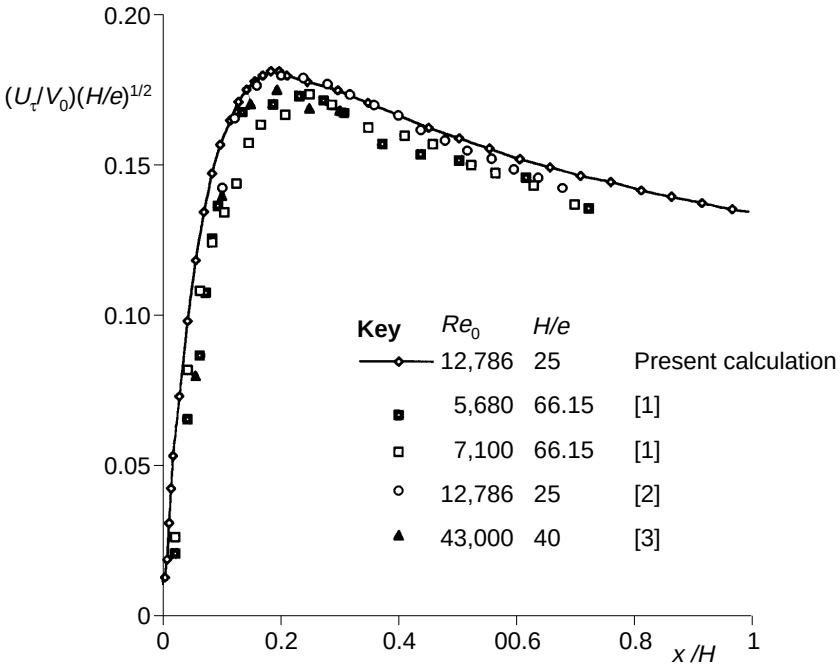

Figure 15.
Non-dimensional friction velocity distributions – comparisons with experimental data

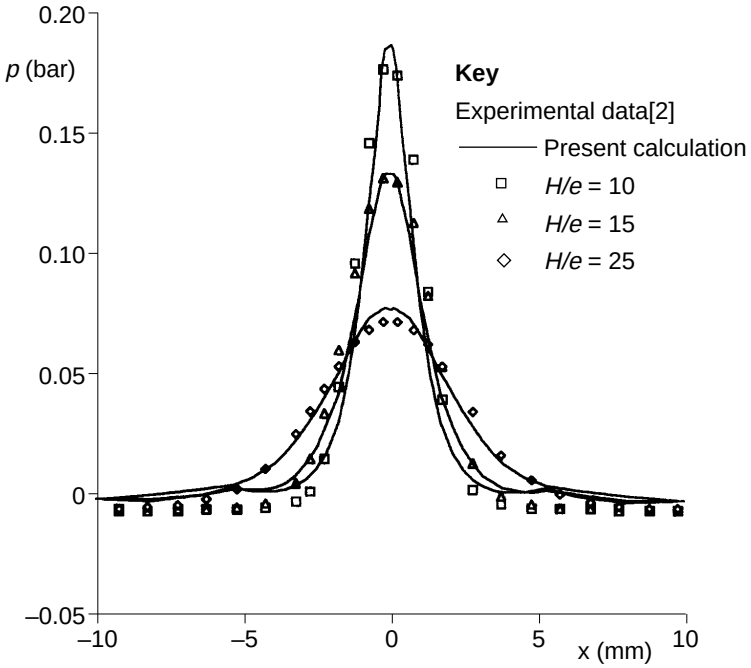

Figure 16.
Wall pressure distributions

was defined by the non-dimensional value y^+ ranging from 20 to 60. Also, a value for the relative distance x/H was defined as the transition between the logarithmic and the generalized laws. The use of the hybrid law provided quite good agreement with experimental data.

References

1. Beltaos, S. and Rajaratnam, N., "Plane turbulent impinging jets", *Journal of Hydraulics Research,* Vol. 1, 1973, pp. 29-59.
2. Mohamed Aly, O.S.M., "Etude d'un jet d'air plan mince a grande vitesse. Action sur une plaque plane", Thèse en Energétique, University of Valenciennes, France, 1993.
3. Shauer, J.J. and Eustis, R.H., "The flow development and heat transfer characteristics of plane turbulent impinging jets", Technical Report 3, Department of Mechanical Engineering, Stanford University, CA, 1963.
4. Childs, R.E. and Dixon, D., "Simulation of impinging turbulent jets", AIAA 23rd Aerospace Sciences Meeting, 14-17 January 1985, Reno, NV.
5. Hwang, C.J. and Liu, J.L., "Numerical study of two-dimensional impinging jet flow fields", *AIAA Journal,* Vol. 27 No. 7, 1989, pp. 841-2.
6. Leschziner, M.A., "Application of second-moment closure in complex flows", VKI Lecture series 1993-02, von Karman Institute for Fluid Dynamics.
7. Looney, M.K. and Walsh, J.J., "Mean flow and turbulent characteristics of free and impinging jet flows", *Journal of Fluid Mechanics*, Vol. 147, 1984, pp. 397-429.
8. Wolfshtein, M., "Some solutions of plane turbulent impinging jets", *Journal of Basic Engineering*, Vol. 12, 1970, pp. 915-22.
9. Harlow, F.H. and Nakayama, P.I., "Transfer of turbulence energy decay rate", Los Alamos Scientific Laboratory, University of California, Ref. LA-3854, 1968.
10. Spalding, D.B., "A turbulence model for buoyant and combusting flows", Imperial College CFDU, Report 86/4, London.
11. Patankar, S.V., *Numerical Heat Transfer and Fluid Flow*, McGraw-Hill, New York, NY, 1980.
12. Mathieu, J., Jeandel, D., Launder, B.E., Reynolds, W.C. and Rodi, W., "La simulation des modèles de turbulence et leurs applications", Ecole d'Été d'Analyse Numérique, CEA-EDF-INRIA, Eyrolles, 1984.
13. Chieng, R.K. and Ng, T.T., "Some aspects of strongly heated turbulent boundary layer flow", *Phys. Fluids,* Vol. 25, 1982, pp. 1333-41.
14. Launder, B.E., "An introduction to single-point closure methodology, introduction to the modelling of turbulence", von Karman Institute of Fluid Dynamics, Lecture Series 1993-02.
15. Schiestel, R., "Modélisation et simulation des écoulements turbulents", *Traité des Nouvelles Technologies*, Série Mécanique, Edition Hermes, Paris, 1993.
16. Bouainouche, M., "Etude de l'interaction entre un jet plan mince à grande vitesse et un film liquide", Thèse en Energétique, University of Valenciennes, France, 1995.
17. Ljuboja, M. and Rodi, W., "Calculation of turbulent wall jets with an algebraic Reynolds stress model", *Transaction of ASME, Journal of Fluids Engineering* Vol. 102, 1980, pp. 350-6.
18. Patel, V.C., "Calibration of Preston tube and limitations on its use in pressure gradients", *Journal of Fluid Mechanics*, Vol. 23, 1965, pp. 185-208.